Global high-resolution fire-sourced PM₂.₅ concentrations for 2000-2023

Yonghang Hu[1#], Chenguang Tian[1#], Xu Yue[1*], Yadong Lei[2], Yang Cao[3], Rongbin Xu[4], Yuming Guo[4]

[1] Jiangsu Key Laboratory of Atmospheric Environment Monitoring and Pollution Control, Collaborative Innovation Center of Atmospheric Environment and Equipment Technology, School of Environmental Science and Engineering, Nanjing University of Information Science & Technology (NUIST), Nanjing 210044, China

[2] State Key Laboratory of Severe Weather & Key Laboratory of Atmospheric Chemistry of CMA, Chinese Academy of Meteorological Sciences, Beijing 100081, China

[3] Jiangsu Nanjing Environmental Monitoring Center, Nanjing 210041, China

[4] Climate, Air Quality Research Unit, School of Public Health and Preventive Medicine, Monash University, Melbourne, Australia

Correspondence to: Xu Yue (yuexu@nuist.edu.cn)

[#] These authors contributed equally to this work.

Abstract. Fires are a significant disturbance in Earth's systems. Smoke aerosols emitted from fires can cause environmental degradation and climatic perturbations, leading to exacerbated air pollution and posing hazards to public health. However, research on the climatic and health impacts of fire emissions is severely limited by the scarcity of air pollution data directly attributed to these emissions. Here, we develop a global daily fire-sourced $PM_{2.5}$ concentration ($[PM_{2.5}]$) dataset at a spatial resolution of 0.25^{o} for the period 2000-2023, using the GEOS-Chem chemical transport model driven with two fire emission inventories, the Global Fire Emissions Database version 4.1 with small fires (GFED4.1s) and the Quick Fire Emission Dataset version 2.5r1 (QFED2.5). Simulated all-source $[PM_{2.5}]$ are bias-corrected using a machine learning algorithm, which incorporates ground observations from over 9000 monitoring sites worldwide. Then the simulated ratios between fire- and all-source $[PM_{2.5}]$ at individual grids are applied to derive fire-sourced $[PM_{2.5}]$. Globally, the average fire-sourced $[PM_{2.5}]$ is estimated to be 1.94 µg m^{-3} with GFED4.1s and 3.74 µg m^{-3} with QFED2.5. Both datasets show consistent spatial distributions with regional hotspots in central Africa and widespread decreasing trends over most areas. While the mean levels of fire-sourced $[PM_{2.5}]$ are much larger at low latitudes, fire episodes at the boreal regions can cause comparable $PM_{2.5}$ levels as in the tropics. This dataset serves as a valuable tool for exploring the impacts of fire-related air pollutants on climate, ecosystems, and public health, enabling accurate assessments and supports for decision-making in environmental management and policy.

1 Introduction

Atmospheric particulate matter, typically PM$_{2.5}$ with aerodynamic diameter less than 2.5 μm, poses
40 significant impacts on air quality, climate system, and public health (Salana et al., 2024;Xie et al.,
2024;Gu et al., 2021). These fine particles originate from a variety of sources, among which the biomass
burning from both natural wildfires and anthropogenic activities makes substantial contributions (Burke
et al., 2023;Connolly et al., 2024;Atuyambe et al., 2024). The fire PM$_{2.5}$ is particularly toxic due to its
chemical composition and smaller size compared to urban-derived PM$_{2.5}$ (Aguilera et al., 2021). Exposure
45 to elevated fire PM$_{2.5}$ has been observed to increase the mortality rates for various diseases, particularly
cardiovascular and respiratory ailments (Chen et al., 2021). Additionally, the increased temperatures
associated with wildfire emissions promote the likelihood of adverse health effects (Xu et al., 2020).
Furthermore, the heterogenous distribution of fire PM$_{2.5}$ concentrations ([PM$_{2.5}$]) poses much larger
population exposure for low-income countries (Xu et al., 2023). Over the past a few decades, the
50 frequency and magnitude of wildfire occurrences have escalated due to climate change and extreme
weather events (Ward et al., 2012;Melia et al., 2022;Zhu et al., 2021;Hu et al., 2024b). Hence, a
comprehensive examination of the trends and influencing factors related to fire PM$_{2.5}$ is important for the
development of effective environmental protection and health policies.

Currently, two principal approaches are used for estimating fire [PM$_{2.5}$] on the large scale (Yue et al.,
55 2024). The first method derives the changes of air pollutants before and after specific fire events using
observational records. For example, Roberts and Wooster (2021) used Copernicus Atmosphere
Monitoring Service, a system integrating remote sensing and ground-based observations, to estimate that
fire air pollutants result in approximately 750,000 deaths annually worldwide with the highest mortality
rates observed in Asia and Africa. Burke et al. (2023) utilized both surface and spaceborne PM$_{2.5}$
60 measurements (from 2000 to 2022) and found that wildfire smoke has stabilized or even reversed the
decreasing trends of [PM$_{2.5}$] in most U.S. states since 2016. Notably, these fire-induced increases are
expected to remain unregulated as the climate continues to warm. In addition to station and satellite
observations, numerical modelling is also a valuable tool to assess [PM$_{2.5}$] from fire emissions. For
instance, Chen et al. (2021) employed the GEOS-Chem model to estimate daily [PM$_{2.5}$] attributable to
65 wildfires and revealed that short-term exposure to fire PM$_{2.5}$ increases mortality risks, especially the all-
cause, cardiovascular, and respiratory deaths. Zhang et al. (2023) utilized an advanced model to assess
daily [PM$_{2.5}$] originating from both fire and non-fire sources across various regions of the USA. Their
findings showed that fire smokes accounted for over 25% of the daily PM$_{2.5}$ levels recorded in the Air
Quality System of Environmental Protection Agency (EPA) from 2007 to 2018, deteriorating the U.S. air
70 quality particularly along the Pacific coast and in the southeast.

However, there are considerable discrepancies in modelled concentrations of wildfire pollutants due
to variations in physicochemical processes, model resolutions, and meteorological forcings (Markakis et
al., 2015;Wolke et al., 2012). Moreover, differences in fire emission inventories can significantly

influence the assessment of fire air pollutants. For example, Desservettaz et al. (2022) used the chemical

75 transport model (CTM) GEOS-Chem and revealed that the Global Fire Emissions Database version 4 with small fires (GFED4s) outperformed other fire inventories in Australia. On the global scale, Pan et al. (2020) used six fire emission inventories to drive GEOS-Chem model and found that simulations using the Quick Fire Emission Dataset (QFED) version 2.4 yielded the closest estimate of aerosol optical depth compared to both site-level and satellite-based observations during fire seasons. These studies revealed

80 certain discrepancies among fire inventories and suggested a need of the comparison among these inventories to improve the accuracy of predicted fire air pollutants.

Due to inherent limitations in CTMs and inventories, there has been a growing utilization of machine learning algorithms in recent years. These algorithms have proven effective in reducing biases in model simulations, particularly in regional analysis and prediction of wildfire pollutant concentrations. For

85 instance, Wei et al. (2019) developed a space-time random forest (RF) algorithm that integrated satellite data, ground observations, and model outputs to estimate daily $PM_{2.5}$ and black carbon concentrations at a one-kilometer resolution across the U.S. during 2000-2020.. On the global scale, Xu et al. (2023) used the RF algorithm to bias-correct the GEOS-Chem output, so as to assess global daily $[PM_{2.5}]$ generated from wildfires during 2001-2019. They improved the determination coefficient of simulated $PM_{2.5}$ from

90 0.22 of the original GEOS-Chem model to 0.75 with the RF adjustment. Their analyses showed that approximately 2.18 billion people experienced at least one day of severe pollution per year due to fire-emitted $PM_{2.5}$, with an average exposure of 9.9 days per person each year. However, due to the large computational cost, most of these machine learning algorithms were applied at the regional scale or driven with single fire inventories, which restricts their ability to accurately quantify the spatiotemporal

95 variability of fire air pollutants.

In this study, the GEOS-Chem model was employed to create two global datasets of fire $[PM_{2.5}]$ corresponding to the GFED4.1s and QFED2.5 emission inventories. These model datasets were refined using the eXtreme Gradient Boosting (XGBoost) machine learning approach in combination with abundant *in situ* measurements from thousands of monitoring stations. Subsequently, two sets of daily

100 fire $PM_{2.5}$ data were generated with temporal coverage from 2000 to 2023 and a fine spatial resolution of 0.25°×0.25°. We aim to systematically compare $[PM_{2.5}]$ across different regions, specifically focusing on the variations in $PM_{2.5}$ levels attributable to fire emissions.

2 Data and methods

2.1 Observations of surface $PM_{2.5}$ concentrations

105 We collected site-level measurements of $[PM_{2.5}]$ from a total of ~9000 monitoring stations in the world. The site number varied year by year with the maximum of 9541 in the year 2022. The data at 1822 sites in China for 2014-2023 were obtained from the China National Environmental Monitoring Center

(CNEMC, http://www.cnemc.cn). For the earlier years (2000-2013), we interpolated the data-fusion product of Tracking Air Pollution (TAP, http://tapdata.org.cn) (Xiao et al., 2021;Geng et al., 2021) to

110   1822 ground stations to align with the CNEMC data. This TAP dataset has shown a good consistency with observed Chinese $PM_{2.5}$ levels for 2015-2022 (Fig. S1). In the United States, $PM_{2.5}$ observations at 1198 sites for 2000-2023 were obtained from the Environmental Protection Agency (EPA, https://www.epa.gov). European $PM_{2.5}$ data at 1687 sites in 2013-2023 were obtained from the European Environment Agency (EEA, https://www.eea.europa.eu/en), with data in pre-2013 coming from the

115   European Monitoring and Evaluation Programme (EMEP, https://emep.int). $PM_{2.5}$ data for other countries at 4995 sites were downloaded from OpenAQ (https://openaq.org) and the World's Air Pollution: Real-time Air Quality Index (https://waqi.info), where the Air Quality Index (AQI) was converted to $PM_{2.5}$ following a standardized methodology. All $PM_{2.5}$ data, both daily and hourly, have undergone rigorous quality checks with outliers removed to ensure accuracy. Daily values were calculated from the hourly

120   data, and sites with fewer than 10-day data in a year were excluded from the analysis. Finally, a total of 2560645 records were compiled for the model training and validation.

2.2 Auxiliary data

The auxiliary data utilized in this study are detailed in Table S1. Climatic data were downloaded from the ECMWF Reanalysis v5 (ERA5, https://www.ecmwf.int/en/forecasts/dataset/ecmwf-reanalysis-v5)

125   with a spatial resolution of 0.25°×0.25° at the hourly interval. Relative humidity was calculated using surface pressure, 2-m temperature, and 2-meter dewpoint, based on the Clausius-Clapeyron equation (Pechony and Shindell, 2009). These meteorological data were aggregated to daily time scale to be consistent with $PM_{2.5}$ measurements. Global land cover data from 2000 to 2023 were obtained from MODIS Land Cover (https://modis-land.gsfc.nasa.gov/landcover.html), which classifies 17 vegetation

130   types according to the International Geosphere-Biosphere Programme (IGBP).

2.3 GEOS-Chem model simulation

We used the GEOS-Chem model (version 12.0.0, https://geoschem.github.io) to predict global $[PM_{2.5}]$ and isolate the contributions from fire emissions. The model is a global three-dimensional CTM operating

135   at a horizontal resolution of 2° latitude by 2.5° longitude with 47 vertical layers extending from ground level to the mesosphere (Lu et al., 2019;David et al., 2019;Yan et al., 2018). The model incorporates MERRA-2 meteorological inputs and implements a comprehensive chemical mechanism covering HOx-NOx-VOCs-O_3-halogen-aerosol interactions (Mao et al., 2013). Previous studies have extensively demonstrated the effectiveness of GEOS-Chem in simulating the reasonable distribution of trace gases

140   and aerosols at multiple spatial and temporal scales (Breider et al., 2014;Li et al., 2019;Xu et al., 2013).

Emissions from various sources, regions, and types are processed using the Harvard–NASA Emissions Component (HEMCO) module, which operates online and allows users to specify the grid, apply scaling factors, and dynamically integrate, overlay, and update emission inventories (Keller et al., 2014). In our study, we incorporated two daily fire emission inventories within the HEMCO framework, including GFED4.1s (short as GFED thereafter) and QFED2.5 (short as QFED thereafter), both of which range from 2000 to 2023 (last modified in June 26th, 2024). All simulated PM$_{2.5}$ data at 2°×2.5° from GEOS-Chem were downscaled to 0.25°×0.25° using the bilinear interpolation (Wei et al., 2021). In addition, we estimated [PM$_{2.5}$] unaffected by fires by disabling the biomass combustion inventories in GEOS-Chem.

2.4 The machine learning algorithm

We used the XGBoost machine learning algorithm to bias-correct the simulated all-source [PM$_{2.5}$]. XGBoost is based on the principle of gradient tree boosting (GTB) algorithms, which combine multiple imperfect decision trees (referred to as base or weak learning trees) to create a more accurate composite decision tree (Chen and Guestrin, 2016). XGBoost is designed for efficiency and speed, capable of building trees gradually and supporting customized objective functions and evaluation metrics. These features make it particularly well-suited for various regression tasks. The primary objective of this algorithm is to minimize of loss function, enhancing the model's predictive accuracy. Notably, XGBoost provides a robust and scalable solution that optimizes computational speed and reduces memory usage when training large sample datasets (Li et al., 2020). The formula for prediction is defined as follows:

$$\hat{Y} = \sum_{k=1}^{K} f_k(X) \tag{1}$$

where $\hat{Y}$ is the predicted daily [PM$_{2.5}$]; X is the input variable related to [PM$_{2.5}$], which includes simulated [PM$_{2.5}$] from GEOS-Chem, meteorological fields, and land cover data (Table S1). K is the number of decision trees used in the model, and f_k denotes the tree constructed to minimize the residuals left by the (k-1)th tree.

XGBoost implements early stopping strategies and regularization techniques within the objective function to effectively prevent overfitting. The kth iteration of XGBoost function (R^k) is defined as follows:

$$R^k = \sum_{i=1}^{t} l\left(y_i, \hat{y}_i^{\ k}\right) + \sum_{j=1}^{k} \Omega\left(f_j\right) \tag{2}$$

where t refers to the number of samples; y_i represents the actual value of the ith sample, and $\hat{y}_i^{\ k}$ means the predicted value of the ith sample after k iterations. The function $l\left(y_i, \hat{y}_i^{\ k}\right)$ is a differentiable loss function used to measure the discrepancy between y_i and $\hat{y}_i^{\ k}$. The regularization term $\Omega\left(f_j\right)$ includes the complexity of the amount of the tree f_j, such as the number of nodes and the weights assigned to each node (Ma et al., 2020). In addition, XGBoost employs a second-order Taylor expansion for the loss

function, enhancing the precision of the model's error assessment and consequently improving the accuracy of predictions (Wong et al., 2021).

175   In this study, we used meteorological data, land cover information, and simulated all-source [PM$_{2.5}$] from the GEOS-Chem model (Table S1) to develop XGBoost models. These gridded input data were interpolated to monitoring sites, and the site-level PM$_{2.5}$ measurements was used as the predictand. Due to the substantial data volume, we trained the XGBoost model on a year-by-year basis using available measurements and modeling data from the corresponding years. For each year, 80% of observational

180 records were randomly selected to train the XGBoost model, while the remaining 20% were used as independent samples for validations. The developed and validated machine learning models were then used to derive global gridded [PM$_{2.5}$], using meteorological reanalyses, land cover data, as well as PM$_{2.5}$ outputs from GEOS-Chem models, at the resolution of 0.25°×0.25° on a daily base. We estimated fire-emitted [PM$_{2.5}$] by applying the simulated fire-to-all ratio of [PM$_{2.5}$] to the XGB-adjusted all-source

185 [PM$_{2.5}$] following the same approach by Xu et al. (2023):

$$[PM_{2.5}]_{fire} = \frac{[PM_{2.5}]_{all}^{GC} - [PM_{2.5}]_{nofire}^{GC}}{[PM_{2.5}]_{all}^{GC}} \times [PM_{2.5}]_{all}^{XBG} \qquad (3)$$

3 Results

3.1 Bias-correction and validation of all-source [PM$_{2.5}$]

    Figure 1 shows the locations of monitoring sites and the corresponding [PM$_{2.5}$] in 2022. High levels

190 of PM$_{2.5}$ are observed in Asia, especially over India and East Asia, where large anthropogenic emissions locate. Predicted all-source [PM$_{2.5}$] by the XGBoost model, which implements GEOS-Chem simulations considering GFED fire emissions, in general captures the observed spatial pattern with the determination coefficient (R^2) of 0.82, a root-mean-square error (RMSE) of 9.22 μg m^{-3}, and a normalized mean bias (NMB) of 0.71%, respectively (Fig. 1b). Similarly, the XGBoost model demonstrates good performance

195 when applied to GEOS-Chem simulations driven with QFED inventory, as shown in Fig. S2 for the results of 2022.

    Figure 2 presents the top ten most crucial features identified by the XGBoost model for predicting all-source [PM$_{2.5}$] using two different fire inventories in 2022. As expected, the data simulated by the GEOS-Chem model consistently rank as the most important feature. This is followed by meteorological

200 variables such 10-meter wind speed, surface pressure, and boundary layer height, which have a significant influence on [PM$_{2.5}$] variations (Wei et al., 2019). Although there are variations in the importance scores of the top ten features between the two inventories, it is evident that meteorological data has a more pronounced impact on [PM$_{2.5}$] compared to land use data.

    Following the same protocol, we developed machine learning models using XGBoost method for

205 other years as well. Each year's model featured distinct parameterization schemes, and we utilized a 10-

fold cross-validation (CV) method to verify the robustness of these models. The statistical indicators, including CV score R^2, overall R^2, and RMSE for the XGBoost procedures over 24 years are displayed in Fig. 3. The R^2 of CV validation remained above 0.85 throughout the study period, demonstrating that the XGBoost model effectively bias-corrected the predicted all-source PM$_{2.5}$ with reasonable spatial

210 coverage and temporal stability. It should be noted that the R^2 gradually decreased after 2012, likely due to the rapid growth in data volume, which may have weakened the correlations (Perry and Dickson, 2018).

3.2 Development and validation of fire [PM$_{2.5}$]

We compare the all-source [PM$_{2.5}$] with ($[PM_{2.5}]_{all}^{XBG}$) and without ($[PM_{2.5}]_{all}^{GC}$) the XGBoost

215 adjustment. Averaged for 24 years, the original simulations exhibit high [PM$_{2.5}$] in North Africa, India, and East Asia, and relatively high values in eastern U.S. and central Europe (Fig. 4a). With the bias-correction, those hotspots are either weakened or shrink (Fig. 4b). Specially, [PM$_{2.5}$] decreases by 28.8% in North Africa, 12.3% in India, 41.7% in East Asia, 27.5% in eastern U.S., and 35.5% in central Europe (Table 1). In contrast, the adjusted [PM$_{2.5}$] tends to increase over the regions with limited anthropogenic

220 perturbations, such as boreal forest, Tibetan Plateau, Australian desert and so on (Fig. 4c). Such discrepancies suggests that the GEOS-Chem model generally underestimates pollution levels in pristine regions (Kim et al., 2015;Protonotariou et al., 2010) and overestimates them in areas with dense pollution (Lei et al., 2021). Similar changes in [PM$_{2.5}$] are found for the simulations using QFED (Fig. S3) fire inventories. It worths noting that changes of [PM$_{2.5}$] varied significantly over some regions among

225 different fire inventories. For example, the bias-corrected [PM$_{2.5}$] decreases by 19.2% in India and 33.6% in eastern U.S. with QFED (Table 1), much larger than those with GFED, suggesting that differences in fire inventories result in certain discrepancies in the regional [PM$_{2.5}$].

We further derive fire-sourced [PM$_{2.5}$] using Equation (3) and validate it for typical fire events during 2018-2022 (Fig. 5). Fire carbon emissions from GFED are used to pinpoint the accurate fire locations for

230 these events (Table S2). The fire-affected sites are determined if their back trajectory cross the fire locations within the three days after occurrence. For example, 55 sites in Canada exhibited abrupt enhancement of [PM$_{2.5}$] more than 5 times above ordinary level around August 15th, 2023. The back trajectory of these sites aligned with the large fire emissions at the western coast during August 13-15 (Fig. S4). Similarly, 94 sites along the eastern coast of Australia were affected by the fire plume transport

235 during December 8-10, 2019 (Fig. S5). Averaged for these 12 events, the correlation coefficient (R) of [PM$_{2.5}$] between observations and simulations increases from 0.16±0.37 without fire emissions to 0.58±0.29 with fire emissions. The NMB is improved from -53.17±25.50% without fire emissions to 10.68±24.96% with fire emissions during the correspondent fire periods. A similar improvement of [PM$_{2.5}$] is achieved with QFED emission inventory for these fire events (Fig. S6).

240

3.3 Spatiotemporal variations of fire-sourced [PM$_{2.5}$]

We examine the spatiotemporal variations of fire [PM$_{2.5}$] derived from the GFED inventory (Fig. 6). Averaged for 2000-2023, fire-sourced [PM$_{2.5}$] shows strong spatial heterogeneity with the highest concentrations in central Africa and secondary hotspots in South America, Southeast Asia, North America, and Siberia. An upward trend in fire-related [PM$_{2.5}$] is found in Siberia and North America, while most other regions show downward trends (Fig. 6b). Predictions using the QFED inventory indicate much higher long-term average fire-related [PM$_{2.5}$] compared to GFED (Table 2), particularly in the Middle East, western Siberia, and eastern South America (Fig. 6c and 6e). The decreasing trend in fire [PM$_{2.5}$] predicted by QFED is even more pronounced than that predicted by GFED in fire-prone regions such as western Siberia, South America, and Australia (Fig. 6d). In contrast, a positive trend is predicted by QFED in eastern China and Europe, where wildfires are typically limited due to the dense population (Bistinas et al., 2014;Knorr et al., 2014). These differences in fire-sourced [PM$_{2.5}$] are mainly due to the discrepancies in fire inventories. In global fire-prone regions, organic carbon (OC) emissions from fires are 51.08-65.18% lower in the GFED inventory compared to the QFED inventory (Fig. 7a). Moreover, the trends in fire emissions are generally more negative or less positive in QFED than in GFED (Fig. 7b). Globally, the average fire-sourced [PM$_{2.5}$] is estimated to be 1.94 µg m^{-3} with GFED and 3.74 µg m^{-3} with QFED (Table 2).

On the long-term mean basis, fire-related [PM$_{2.5}$] is significantly higher in the tropics than in boreal regions (Fig. 6), primarily due to the high fire emissions in central Africa (Fig. 7). However, during extreme events, fire-sourced [PM$_{2.5}$] can reach comparable levels at both low and high latitudes (Fig. 8). For instance, an unprecedented fire event over Canada in 2023 resulted in a regional hotspot exceeding 30 µg m^{-3}, surpassing the maximum value of ~20 µg m^{-3} in central Africa. Similarly, the extreme Siberian fires in 2019 significantly elevated local [PM$_{2.5}$] and resulted in air pollution levels comparable to those in South America. In the vast tropical areas, fires are primarily driven by anthropogenic activities (Marques et al., 2021;Ward et al., 2018), leading to relatively stable emissions from year to year. In contrast, most biomass burning in boreal regions is caused by wildfires, which are less inhibited by human activities. These uncontrolled fire episodes, combined with the huge carbon storage in boreal forests, result in tremendous emissions in specific years, significantly affecting air quality, climate system, and ecosystem functions at high latitudes in the Northern Hemisphere. It worths noting that fire-sourced [PM$_{2.5}$] shows lower extreme values in QFED (Fig. S7) compared to those in GFED (Fig. 8) over Canada, though the mean fire [PM$_{2.5}$] is much higher associated with the former inventory (Fig. 7).

4 Conclusions and discussion

We developed a global high-resolution dataset of fire-sourced PM$_{2.5}$ concentrations for the period of 2000-2023, using a chemical transport model driven with two fire inventories. A machine learning algorithm was applied to correct biases in the simulated [PM$_{2.5}$] from the GEOS-Chem model, and to

enhance the spatial resolution of data product. Validations demonstrated its high accuracy in capturing all-sourced [PM$_{2.5}$] across more than 9000 global sites and the fire-sourced [PM$_{2.5}$] for typical fire events. Though with some discrepancies, fire-sourced [PM$_{2.5}$] from the two inventories displayed a consistent

280 spatial pattern, with high levels of fire-related air pollution in tropics and relatively lower concentrations at middle to high latitudes. They also exhibited significant global declines in fire-sourced [PM$_{2.5}$] over time, with the most pronounced decreases occurring in tropical regions. In contrast, fire episodes in boreal regions led to stronger enhancement of [PM$_{2.5}$] compared to those in the tropics, due to the larger fuel loads of northern forests and the uncontrolled scale of fires in these areas.

285 Recent advancements in ground monitoring networks and satellite observation systems have led to the development of high-resolution, long-term benchmark datasets for air pollutants (Wei et al., 2023;Gui et al., 2020;Song et al., 2022;Wang et al., 2023;Xiao et al., 2022). However, these datasets typically retrieve total amount of PM$_{2.5}$ without isolating the concentrations specifically caused by fire events. To accurately derive fire-related [PM$_{2.5}$], it is crucial to firstly estimate PM$_{2.5}$ concentrations that are

290 unaffected by fires. Some studies have identified fire-affected sites using satellite imagery and then obtained non-fire PM$_{2.5}$ either by taking the median [PM$_{2.5}$] during non-fire seasons or by using data at nearby sites outside the influence of fire plumes (Burke et al., 2023;Delp and Singer, 2020;O'Dell et al., 2019). This approach, however, depends heavily on the accuracy of high-frequency fire tracking systems to correctly identify fire periods and affected areas. Additionally, it may introduce biases due to not

295 accounting for baseline [PM$_{2.5}$] differences across various locations or periods. In our study, we performed sensitivity experiments using a CTM, where fire emissions were selectively activated or deactivated. This allowed us to more accurately quantify the changes of [PM$_{2.5}$] attributable to fire emissions. Furthermore, we employed machine-learning adjustments to minimize biases inherent in chemical models, thereby improving the accuracy and resolution of the derived fire-related [PM$_{2.5}$].

300 The two datasets derived from different inventories showed discrepancies in both the long-term mean and trend of fire-sourced [PM$_{2.5}$] (Fig. 6). In general, fire-related [PM$_{2.5}$] is much higher when using the QFED inventory compared to GFED, but the long-term trend is more negative with QFED. As expected, these discrepancies can be attributed to differences in the underlying fire emission inventories (Fig. 7). Further validations showed that all-source [PM$_{2.5}$] using GFED yielded an R value of 0.58±0.29 and an

305 NMB of 10.68±24.96% averaged for the 12 fire episodes (Fig. 5). Slightly improved statistical metrics were achieved using QFED, with an R value of 0.63±0.26 and an NMB of 6.56±27.61% for the same events (Fig. S6). However, these differences are too minor to conclusively determine which dataset provides a better estimate of fire-sourced [PM$_{2.5}$]. Fire-sourced [PM$_{2.5}$] is generally lower in the GFED dataset compared to QFED; exceptions exist, such as the 2023 Canadian fires, in which fire-sourced

310 [PM$_{2.5}$] from GFED (Fig. 8) was significantly higher than that from QFED (Fig. S7). Therefore, we recommend using fire-sourced [PM$_{2.5}$] from both inventories jointly to better capture the uncertainties associated with fire-related air pollutants.

There are some uncertainties and limitations in our study. First, the PM$_{2.5}$ observations used for machine learning lack broad spatial coverage. Although we gathered data from thousands of monitoring sites worldwide, most of them are located in the middle to high latitudes of the Northern Hemisphere. PM$_{2.5}$ records are limited in the fire-prone regions, such as central Africa, which are usually wildland areas far away from populated regions. This uneven distribution of monitoring sites may introduce some biases in the derived all-source [PM$_{2.5}$] estimates and the subsequent contributions by fire emissions. Second, we used only one machine learning method for data training. In the preliminary stages, we compared the effectiveness of three different machine learning approaches for correcting biases in simulated [PM$_{2.5}$]. We found that XGBoost algorithm outperformed the other two methods, Random Forest and Deep Neural Networks, showing better statistical metrics against observations (not shown). Although we chose XGBoost for the final analyses, further investigation into results from other machine learning algorithms is warranted to reduce uncertainties inherent in data-driven methods.

Despite the limitations mentioned, our study presents a significant advancement in the development of global daily fire-sourced [PM$_{2.5}$] datasets, featuring the most up-to-date, fine spatial resolution, and covering the longest time period available. By integrating a chemical model with a machine learning approach, we have effectively isolated the impact of fire emissions on ground-level [PM$_{2.5}$], while also addressing and reducing modeling biases. This methodology allows for a more accurate representation of fire-related air pollution. Furthermore, we provide results derived from two different emission inventories, offering a comparison that highlights the uncertainties associated with varying emission estimates. The dataset we have constructed is not only a novel contribution to the field but also holds significant value for future research. It can serve as a critical input for studies examining the climatic, ecological, and epidemiological impacts of air pollutants from global fires. The insights gained from this dataset can inform policy decisions, improve public health strategies, and enhance our understanding of the broader environmental effects of wildfire emissions.

Data availability. The daily fire-sourced [PM$_{2.5}$] from GFED4.1s and QFED2.5 for 2018-2022 are available at https://doi.org/10.5281/zenodo.13380164 (Hu et al., 2024a). The full dataset will be publicly available after the publication of this study.

Author contributions. XY conceived the study. XY, CT and YH designed the research. YH performed the model runs, completed data analysis, and wrote the draft. XY reviewed and edited the manuscript. YL, YC, RX, and YG helped with methods. All authors contributed to the discussion of the results and to the finalization of the paper.

Financial support. This study was jointly supported by the National Key Research and Development Program of China (no. 2023YFF0805402) and Jiangsu Funding Program for Excellent Postdoctoral Talent (no. 2023ZB113).

350

Competing interests. The contact author has declared that none of the authors has any competing interests.

References

Aguilera, R., Corringham, T., Gershunov, A., and Benmarhnia, T.: Wildfire smoke impacts respiratory health more than fine particles from other sources: observational evidence from Southern California, Nature Communications, 12, 1493, https://doi.org/10.1038/s41467-021-21708-0, 2021.

Atuyambe, L. M., Etajak, S., Walyawula, F., Kasasa, S., Nyabigambo, A., Bazeyo, W., Wipfli, H., Samet, J. M., and Berhane, K. T.: Air quality and attributable mortality among city dwellers in Kampala, Uganda: results from 4 years of continuous $PM_{2.5}$ concentration monitoring using BAM 1022 reference instrument, Journal of Exposure Science & Environmental Epidemiology, https://doi.org/10.1038/s41370-024-00684-9, 2024.

Bistinas, I., Harrison, S. P., Prentice, I. C., and Pereira, J. M. C.: Causal relationships versus emergent patterns in the global controls of fire frequency, Biogeosciences, 11, 5087-5101, https://doi.org/10.5194/bg-11-5087-2014, 2014.

Breider, T. J., Mickley, L. J., Jacob, D. J., Wang, Q., Fisher, J. A., Chang, R. Y. W., and Alexander, B.: Annual distributions and sources of Arctic aerosol components, aerosol optical depth, and aerosol absorption, Journal of Geophysical Research: Atmospheres, 119, 4107-4124, https://doi.org/10.1002/2013JD020996, 2014.

Burke, M., Childs, M. L., de la Cuesta, B., Qiu, M., Li, J., Gould, C. F., Heft-Neal, S., and Wara, M.: The contribution of wildfire to $PM_{2.5}$ trends in the USA, Nature, 622, 761-766, https://doi.org/10.1038/s41586-023-06522-6, 2023.

Chen, G., Guo, Y., Yue, X., Tong, S., Gasparrini, A., Bell, M. L., Armstrong, B., Schwartz, J., Jaakkola, J. J. K., Zanobetti, A., Lavigne, E., Nascimento Saldiva, P. H., Kan, H., Royé, D., Milojevic, A., Overcenco, A., Urban, A., Schneider, A., Entezari, A., Vicedo-Cabrera, A. M., Zeka, A., Tobias, A., Nunes, B., Alahmad, B., Forsberg, B., Pan, S.-C., Íñiguez, C., Ameling, C., De la Cruz Valencia, C., Åström, C., Houthuijs, D., Van Dung, D., Samoli, E., Mayvaneh, F., Sera, F., Carrasco-Escobar, G., Lei, Y., Orru, H., Kim, H., Holobaca, I.-H., Kyselý, J., Teixeira, J. P., Madureira, J., Katsouyanni, K., Hurtado-Díaz, M., Maasikmets, M., Ragettli, M. S., Hashizume, M., Stafoggia, M., Pascal, M., Scortichini, M., de Sousa Zanotti Stagliorio Coélho, M., Valdés Ortega, N., Ryti, N. R. I., Scovronick, N., Matus, P., Goodman, P., Garland, R. M., Abrutzky, R., Garcia, S. O., Rao, S., Fratianni, S., Dang, T. N., Colistro, V., Huber, V., Lee, W., Seposo, X., Honda, Y., Guo, Y. L., Ye, T., Yu, W., Abramson, M. J., Samet, J. M., and Li, S.: Mortality risk attributable to wildfire-related $PM_{2.5}$ pollution: a global time series study in 749 locations, The Lancet Planetary Health, 5, e579-e587, https://doi.org/10.1016/S2542-5196(21)00200-X, 2021.

Chen, T., and Guestrin, C.: XGBoost: A Scalable Tree Boosting System, Proceedings of the 22nd ACM SIGKDD International Conference on Knowledge Discovery and Data Mining, San Francisco, California, USA, 2016.

Connolly, R., Marlier, M. E., Garcia-Gonzales, D. A., Wilkins, J., Su, J., Bekker, C., Jung, J., Bonilla, E., Burnett, R. T., Zhu, Y., and Jerrett, M.: Mortality attributable to $PM_{2.5}$ from wildland fires in California from 2008 to 2018, Science Advances, 10, eadl1252, https://doi.org/10.1126/sciadv.adl1252, 2024.

David, L. M., Ravishankara, A. R., Brewer, J. F., Sauvage, B., Thouret, V., Venkataramani, S., and Sinha, V.: Tropospheric ozone over the Indian subcontinent from 2000 to 2015: Data set and simulation using GEOS-Chem chemical transport model, Atmospheric Environment, 219, 117039, https://doi.org/10.1016/j.atmosenv.2019.117039, 2019.

Delp, W. W., and Singer, B. C.: Wildfire Smoke Adjustment Factors for Low-Cost and Professional $PM_{2.5}$ Monitors with Optical Sensors, Sensors, 20, 3683, https://doi.org/10.3390/s20133683, 2020.

Desservettaz, M. J., Fisher, J. A., Luhar, A. K., Woodhouse, M. T., Bukosa, B., Buchholz, R. R., Wiedinmyer, C., Griffith, D. W. T., Krummel, P. B., Jones, N. B., Deutscher, N. M., and Greenslade, J. W.: Australian Fire Emissions of Carbon Monoxide Estimated by Global Biomass Burning Inventories: Variability and Observational Constraints, Journal of Geophysical Research: Atmospheres, 127, e2021JD035925, https://doi.org/10.1029/2021JD035925, 2022.

Geng, G., Xiao, Q., Liu, S., Liu, X., Cheng, J., Zheng, Y., Xue, T., Tong, D., Zheng, B., Peng, Y., Huang, X., He, K., and Zhang, Q.: Tracking Air Pollution in China: Near Real-Time $PM_{2.5}$ Retrievals from Multisource Data Fusion, Environmental Science & Technology, 55, 12106-12115, https://doi.org/10.1021/acs.est.1c01863, 2021.

Gu, B., Zhang, L., Van Dingenen, R., Vieno, M., Van Grinsven, H. J. M., Zhang, X., Zhang, S., Chen, Y., Wang, S., Ren, C., Rao, S., Holland, M., Winiwarter, W., Chen, D., Xu, J., and Sutton, M. A.: Abating ammonia is more cost-effective than nitrogen oxides for mitigating $PM_{2.5}$ air pollution, Science, 374, 758-762, https://doi.org/10.1126/science.abf8623, 2021.

Gui, K., Che, H., Zeng, Z., Wang, Y., Zhai, S., Wang, Z., Luo, M., Zhang, L., Liao, T., Zhao, H., Li, L., Zheng, Y., and Zhang, X.: Construction of a virtual $PM_{2.5}$ observation network in China based on high-density surface meteorological observations using the Extreme Gradient Boosting model, Environment International, 141, 105801, https://doi.org/10.1016/j.envint.2020.105801, 2020.

Hu, Y., Tian, C., and Yue, X.: GFED&QFED: Fire-sourced PM2.5 concentrations dataset (2018-2022), in, https://doi.org/10.5281/zenodo.13380164, 2024a.

Hu, Y., Yue, X., and Tian, C.: Climatic drivers of the Canadian wildfire episode in 2023, Atmospheric and Oceanic Science Letters, 17, 100483, https://doi.org/10.1016/j.aosl.2024.100483, 2024b.

Keller, C. A., Long, M. S., Yantosca, R. M., Da Silva, A. M., Pawson, S., and Jacob, D. J.: HEMCO v1.0: a versatile, ESMF-compliant component for calculating emissions in atmospheric models, Geosci. Model Dev., 7, 1409-1417, https://doi.org/10.5194/gmd-7-1409-2014, 2014.

Kim, P. S., Jacob, D. J., Fisher, J. A., Travis, K., Yu, K., Zhu, L., Yantosca, R. M., Sulprizio, M. P., Jimenez, J. L., Campuzano-Jost, P., Froyd, K. D., Liao, J., Hair, J. W., Fenn, M. A., Butler, C. F., Wagner, N. L., Gordon, T. D., Welti, A., Wennberg, P. O., Crounse, J. D., St. Clair, J. M., Teng, A. P., Millet, D. B., Schwarz, J. P., Markovic, M. Z., and Perring, A. E.: Sources, seasonality, and trends of southeast US aerosol: an integrated analysis of surface, aircraft, and satellite observations with the GEOS-Chem chemical transport model, Atmos. Chem. Phys., 15, 10411-10433, https://doi.org/10.5194/acp-15-10411-2015, 2015.

Knorr, W., Kaminski, T., Arneth, A., and Weber, U.: Impact of human population density on fire frequency at the global scale, Biogeosciences, 11, 1085-1102, https://doi.org/10.5194/bg-11-1085-2014, 2014.

Lei, Y., Yue, X., Liao, H., Zhang, L., Yang, Y., Zhou, H., Tian, C., Gong, C., Ma, Y., Gao, L., and Cao, Y.: Indirect contributions of global fires to surface ozone through ozone–vegetation feedback, Atmos. Chem. Phys., 21, 11531-11543, https://doi.org/10.5194/acp-21-11531-2021, 2021.

Li, S., Zhang, L., Cai, K., Ge, W., and Zhang, X.: Comparisons of the vertical distributions of aerosols in the CALIPSO and GEOS-Chem datasets in China, Atmospheric Environment: X, 3, 100036, https://doi.org/10.1016/j.aeaoa.2019.100036, 2019.

Li, Y., Li, M., Li, C., and Liu, Z.: Forest aboveground biomass estimation using Landsat 8 and Sentinel-1A data with machine learning algorithms, Scientific Reports, 10, 9952, https://doi.org/10.1038/s41598-020-67024-3, 2020.

Lu, X., Zhang, L., Chen, Y., Zhou, M., Zheng, B., Li, K., Liu, Y., Lin, J., Fu, T. M., and Zhang, Q.: Exploring 2016–2017 surface ozone pollution over China: source contributions and meteorological influences, Atmos. Chem. Phys., 19, 8339-8361, https://doi.org/10.5194/acp-19-8339-2019, 2019.

Ma, J., Cheng, J. C. P., Xu, Z., Chen, K., Lin, C., and Jiang, F.: Identification of the most influential areas for air pollution control using XGBoost and Grid Importance Rank, Journal of Cleaner Production, 274, 122835, https://doi.org/10.1016/j.jclepro.2020.122835, 2020.

Mao, J., Paulot, F., Jacob, D. J., Cohen, R. C., Crounse, J. D., Wennberg, P. O., Keller, C. A., Hudman, R. C., Barkley, M. P., and Horowitz, L. W.: Ozone and organic nitrates over the eastern United States: Sensitivity to isoprene chemistry, Journal of Geophysical Research: Atmospheres, 118, 11256-11268, https://doi.org/10.1002/jgrd.50817, 2013.

Markakis, K., Valari, M., Perrussel, O., Sanchez, O., and Honore, C.: Climate-forced air-quality modeling at the urban scale: sensitivity to model resolution, emissions and meteorology, Atmos. Chem. Phys., 15, 7703-7723, https://doi.org/10.5194/acp-15-7703-2015, 2015.

Marques, J. F., Alves, M. B., Silveira, C. F., Amaral e Silva, A., Silva, T. A., dos Santos, V. J., and Calijuri, M. L.: Fires dynamics in the Pantanal: Impacts of anthropogenic activities and climate change, Journal of Environmental Management, 299, 113586, https://doi.org/10.1016/j.jenvman.2021.113586, 2021.

Melia, N., Dean, S., Pearce, H. G., Harrington, L., Frame, D. J., and Strand, T.: Aotearoa New Zealand's 21st-Century Wildfire Climate, Earth's Future, 10, e2022EF002853, https://doi.org/10.1029/2022EF002853, 2022.

O'Dell, K., Ford, B., Fischer, E. V., and Pierce, J. R.: Contribution of Wildland-Fire Smoke to US PM$_{2.5}$ and Its Influence on Recent Trends, Environmental Science & Technology, 53, 1797-1804, https://doi.org/10.1021/acs.est.8b05430, 2019.

Pan, X., Ichoku, C., Chin, M., Bian, H., Darmenov, A., Colarco, P., Ellison, L., Kucsera, T., da Silva, A., Wang, J., Oda, T., and Cui, G.: Six global biomass burning emission datasets: intercomparison and application in one global aerosol model, Atmos. Chem. Phys., 20, 969-994, https://doi.org/10.5194/acp-20-969-2020, 2020.

Pechony, O., and Shindell, D. T.: Fire parameterization on a global scale, Journal of Geophysical Research: Atmospheres, 114, https://doi.org/10.1029/2009JD011927, 2009.

Perry, G. L. W., and Dickson, M. E.: Using Machine Learning to Predict Geomorphic Disturbance: The Effects of Sample Size, Sample Prevalence, and Sampling Strategy, Journal of Geophysical Research: Earth Surface, 123, 2954-2970, https://doi.org/10.1029/2018JF004640, 2018.

Protonotariou, A., Tombrou, M., Giannakopoulos, C., Kostopoulou, E., and Le Sager, P.: Study of CO surface pollution in Europe based on observations and nested-grid applications of GEOS-CHEM global chemical transport model, Tellus B: Chemical and Physical Meteorology, 62, 209-227, https://doi.org/10.1111/j.1600-0889.2010.00462.x, 2010.

Roberts, G., and Wooster, M. J.: Global impact of landscape fire emissions on surface level PM$_{2.5}$ concentrations, air quality exposure and population mortality, Atmospheric Environment, 252, 118210, https://doi.org/10.1016/j.atmosenv.2021.118210, 2021.

Salana, S., Yu, H., Dai, Z., Subramanian, P. S. G., Puthussery, J. V., Wang, Y., Singh, A., Pope, F. D., Leiva G, M. A., Rastogi, N., Tripathi, S. N., Weber, R. J., and Verma, V.: Inter-continental variability in the relationship of oxidative potential and cytotoxicity with PM$_{2.5}$ mass, Nature Communications, 15, 5263, https://doi.org/10.1038/s41467-024-49649-4, 2024.

Song, Z., Chen, B., Zhang, P., Guan, X., Wang, X., Ge, J., Hu, X., Zhang, X., and Wang, Y.: High temporal and spatial resolution PM$_{2.5}$ dataset acquisition and pollution assessment based on FY-4A TOAR data and deep forest model in China, Atmospheric Research, 274, 106199, https://doi.org/10.1016/j.atmosres.2022.106199, 2022.

Wang, L., Liu, B., Li, R., Chen, X., Liu, L., Tang, X., Liu, J., Liao, Z., Xin, J., Wang, Y., and Hu, B.: Prediction of daily PM$_{2.5}$ and ozone based on high-density weather stations in China: Nonlinear effects of meteorology, human and ecosystem health risks, Atmospheric Research, 293, 106889, https://doi.org/10.1016/j.atmosres.2023.106889, 2023.

Ward, D. S., Kloster, S., Mahowald, N. M., Rogers, B. M., Randerson, J. T., and Hess, P. G.: The changing radiative forcing of fires: global model estimates for past, present and future, Atmos. Chem. Phys., 12, 10857-10886, https://doi.org/10.5194/acp-12-10857-2012, 2012.

Ward, D. S., Shevliakova, E., Malyshev, S., and Rabin, S.: Trends and Variability of Global Fire Emissions Due To Historical Anthropogenic Activities, Global Biogeochemical Cycles, 32, 122-142, https://doi.org/10.1002/2017gb005787, 2018.

Wei, J., Huang, W., Li, Z., Xue, W., Peng, Y., Sun, L., and Cribb, M.: Estimating 1-km-resolution PM$_{2.5}$ concentrations across China using the space-time random forest approach, Remote Sensing of Environment, 231, 111221, https://doi.org/10.1016/j.rse.2019.111221, 2019.

Wei, J., Li, Z., Lyapustin, A. I., Sun, L., Peng, Y., Xue, W., Su, T., and Cribb, M.: Reconstructing 1-km-resolution high-quality PM$_{2.5}$ data records from 2000 to 2018 in China: spatiotemporal variations and policy implications, Remote Sensing of Environment, 252, 112136, https://doi.org/10.1016/j.rse.2020.112136, 2021.

Wei, J., Li, Z., Lyapustin, A., Wang, J., Dubovik, O., Schwartz, J., Sun, L., Li, C., Liu, S., and Zhu, T.: First close insight into global daily gapless 1 km PM$_{2.5}$ pollution, variability, and health impact, Nature Communications, 14, 8349, https://doi.org/10.1038/s41467-023-43862-3, 2023.

Wolke, R., Schröder, W., Schrödner, R., and Renner, E.: Influence of grid resolution and meteorological forcing on simulated European air quality: A sensitivity study with the modeling system COSMO–MUSCAT, Atmospheric Environment, 53, 110-130, https://doi.org/10.1016/j.atmosenv.2012.02.085, 2012.

Wong, P.-Y., Lee, H.-Y., Chen, Y.-C., Zeng, Y.-T., Chern, Y.-R., Chen, N.-T., Candice Lung, S.-C., Su, H.-J., and Wu, C.-D.: Using a land use regression model with machine learning to estimate ground level PM$_{2.5}$, Environmental Pollution, 277, 116846, https://doi.org/10.1016/j.envpol.2021.116846, 2021.

Xiao, Q., Geng, G., Cheng, J., Liang, F., Li, R., Meng, X., Xue, T., Huang, X., Kan, H., Zhang, Q., and He, K.: Evaluation of gap-filling approaches in satellite-based daily PM$_{2.5}$ prediction models, Atmospheric Environment, 244, 117921, https://doi.org/10.1016/j.atmosenv.2020.117921, 2021.

Xiao, Y., Wang, Y., Yuan, Q., He, J., and Zhang, L.: Generating a long-term (2003−2020) hourly 0.25° global PM$_{2.5}$ dataset via spatiotemporal downscaling of CAMS with deep learning (DeepCAMS), Science of The Total Environment, 848, 157747, https://doi.org/10.1016/j.scitotenv.2022.157747, 2022.

Xie, Y., Zhou, M., Hunt, K. M. R., and Mauzerall, D. L.: Recent PM$_{2.5}$ air quality improvements in India benefited from meteorological variation, Nature Sustainability, https://doi.org/10.1038/s41893-024-01366-y, 2024.

Xu, R., Yu, P., Abramson, M. J., Johnston, F. H., Samet, J. M., Bell, M. L., Haines, A., Ebi, K. L., Li, S., and Guo, Y.: Wildfires, Global Climate Change, and Human Health, New England Journal of Medicine, 383, 2173-2181, https://doi.org/10.1056/NEJMsr2028985, 2020.

Xu, R., Ye, T., Yue, X., Yang, Z., Yu, W., Zhang, Y., Bell, M. L., Morawska, L., Yu, P., Zhang, Y., Wu, Y., Liu, Y., Johnston, F., Lei, Y., Abramson, M. J., Guo, Y., and Li, S.: Global population exposure to landscape fire air pollution from 2000 to 2019, Nature, 621, 521-529, https://doi.org/10.1038/s41586-023-06398-6, 2023.

495   Xu, X., Wang, J., Henze, D. K., Qu, W., and Kopacz, M.: Constraints on aerosol sources using GEOS-Chem adjoint and MODIS radiances, and evaluation with multisensor (OMI, MISR) data, Journal of Geophysical Research: Atmospheres, 118, 6396-6413, https://doi.org/10.1002/jgrd.50515, 2013.

Yan, Y., Lin, J., and He, C.: Ozone trends over the United States at different times of day, Atmos. Chem. Phys., 18, 1185-1202, https://doi.org/10.5194/acp-18-1185-2018, 2018.

500   Yue, X., Hu, Y., Tian, C., Xu, R., Yu, W., and Guo, Y.: Increasing impacts of fire air pollution on public and ecosystem health, The Innovation, 5, 100609, https://doi.org/10.1016/j.xinn.2024.100609, 2024.

Zhang, D., Wang, W., Xi, Y., Bi, J., Hang, Y., Zhu, Q., Pu, Q., Chang, H., and Liu, Y.: Wildland Fires Worsened Population Exposure to $PM_{2.5}$ Pollution in the Contiguous United States, Environmental Science & Technology, 57, 19990-19998, https://doi.org/10.1021/acs.est.3c05143, 2023.

505   Zhu, A., Xu, H., Deng, J., Ma, J., and Li, S.: El Niño–Southern Oscillation (ENSO) effect on interannual variability in spring aerosols over East Asia, Atmos. Chem. Phys., 21, 5919-5933, https://doi.org/10.5194/acp-21-5919-2021, 2021.
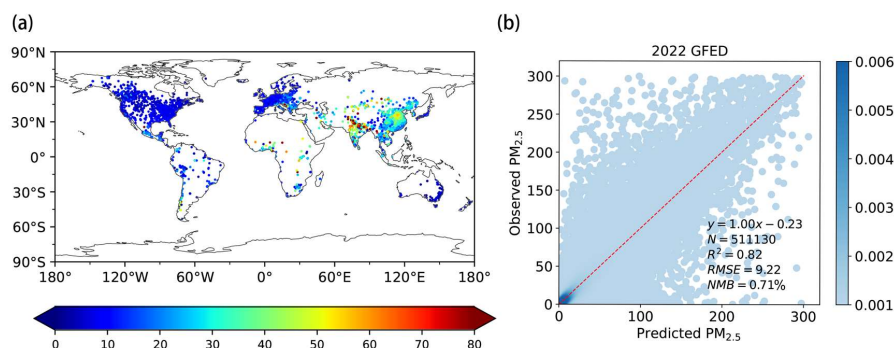
510 **Figure 1.** Observed PM$_{2.5}$ concentrations and their comparisons with predictions made by the XGBoost model. Panel (a) presents the annual mean PM$_{2.5}$ concentrations (µg m^{-3}) at 9541 monitoring sites in 2022. Panel (b) shows daily PM$_{2.5}$ concentrations predicted by the GEOS-Chem model, adjusted using the XGBoost approach, and compared with validation subsets of observations in 2022. The GEOS-Chem simulations incorporate emissions from both anthropogenic sources and the Global Fire Emissions Database version 4.1s. Colors in (b) represent data frequency, and the red dashed line indicates the

515 linear regression. Validation metrics, including the sample size (N, 20% of total observational records), regression equation, determination coefficient (R^2), root-mean-square error (RMSE), and normalized mean bias (NMB), are provided. GEOS-Chem simulations using QFED inventory for 2022 are shown in Fig. S2.
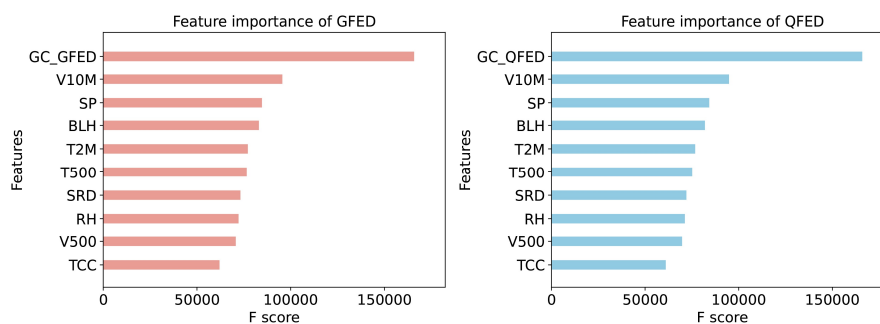
520

Figure 2. Top 10 important features measured by F-score for the machine learning model, which was trained using GEOS-Chem simulations with fire emissions from (a) GFED and (b) QFED inventories in 2022, respectively. The full name of each feature is shown in Table S1.

525
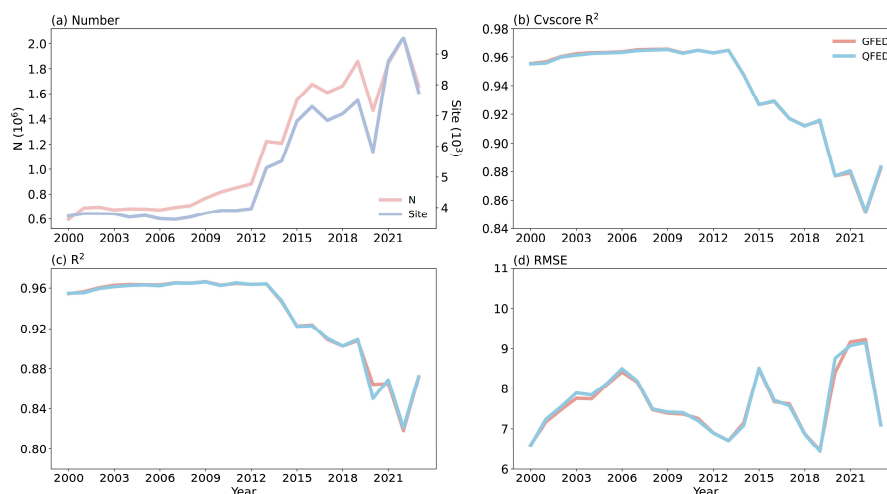
Figure 3. Statistical metrics of simulated PM$_{2.5}$ concentrations ([PM$_{2.5}$]) from 2000 to 2023. Panel (a) shows the total number of sites and samples (N) used for machine learning training. Panel (b) presents the 10-fold cross-validation R^2 for each year, comparing simulations using different fire emission inventories, including GFED and QFED. Panels (c) and (d) display the 530 year-to-year R^2 and RMSE between observed and simulated [PM$_{2.5}$] using these different fire emission inventories.
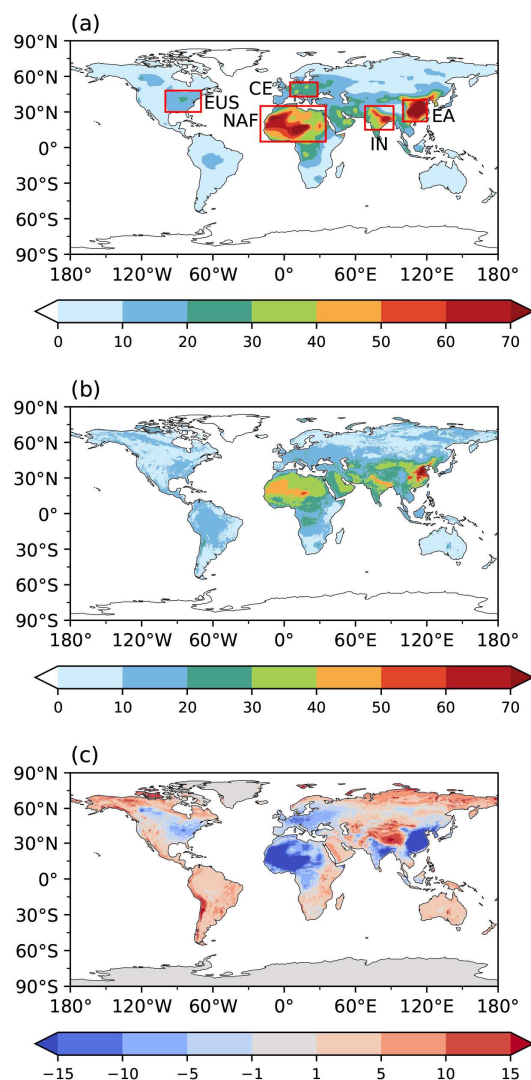
Figure 4. Annual mean all-source [PM$_{2.5}$] for 2000-2023 from the (a) original GEOS-Chem simulations at 0.25°×0.25º resolution and (b) bias-corrected simulations using the XGBoost approach at the same resolution. The difference between the original and bias-corrected [PM$_{2.5}$] is shown in (c). The simulated [PM$_{2.5}$] is derived using GFED4s fire emissions.
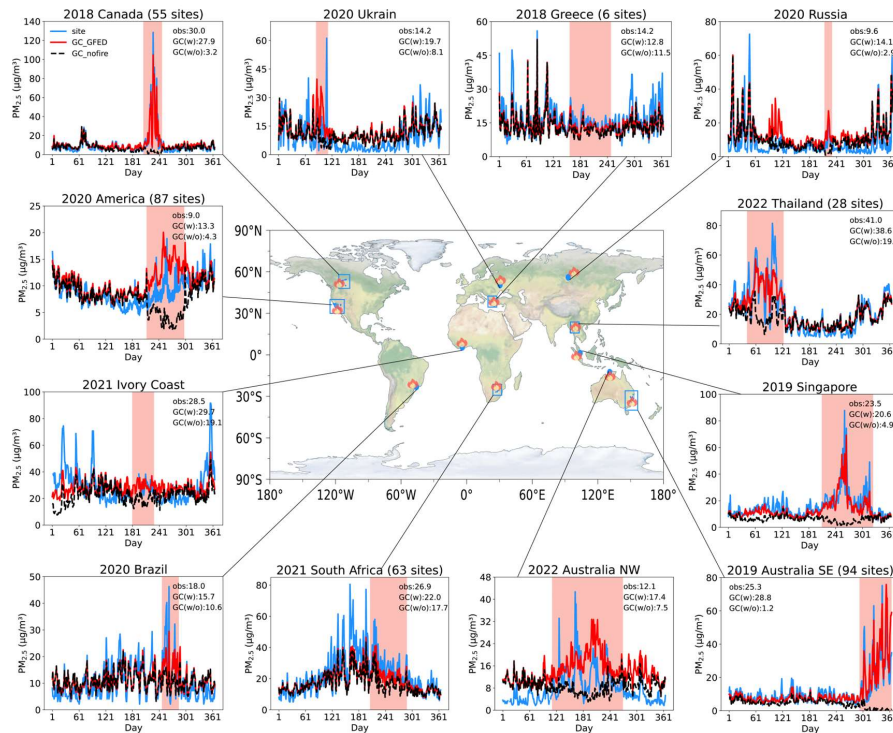
Figure 5. Comparisons of [PM$_{2.5}$] between observations (blue) and simulations with (red) and without (black) fire emissions for 12 incidences during 2018-2022. The simulations are performed using the GEOS-Chem model driven with fire emissions from the GFED inventory and bias-corrected with the XGBoost approach. Blue boxes (representing multiple sites) or points (representing single sites) on the map indicate the locations of air quality monitoring sites affected by nearby fire plumes. The sources of these fire episodes were determined using Lagrangian back-trajectory analysis as shown in Figs S4-S5. The observed and simulated [PM$_{2.5}$] at all sites averaged for fire periods are shown on each panel. These fire events were sourced from the Global Disaster Data Platform (https://www.gddat.cn/newGlobalWeb), which provides fire locations and the approximate start and end dates as shown in Table S2.
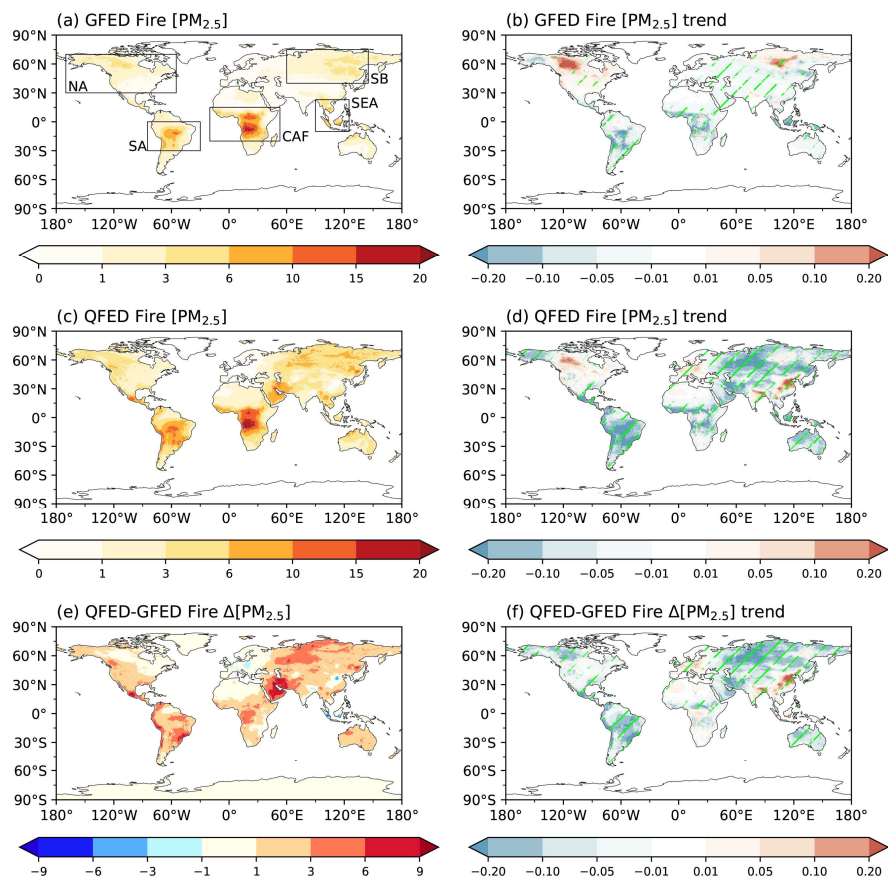
Figure 6. Long-term (a) mean and (b) trend of fire [PM$_{2.5}$] derived using the GFED inventory for 2000-2023. The box regions in (a) indicate areas used for comparing differences between two inventories. Panels (c) and (d) display the same information as (a) and (b), but for fire [PM$_{2.5}$] from QFED inventory. The differences in fire [PM$_{2.5}$] (Δ[PM$_{2.5}$]) between the two inventories are presented for the long-term (e) mean and (f) trend during 2000-2023. Green slashes indicate areas with significant ($p < 0.05$) changes.
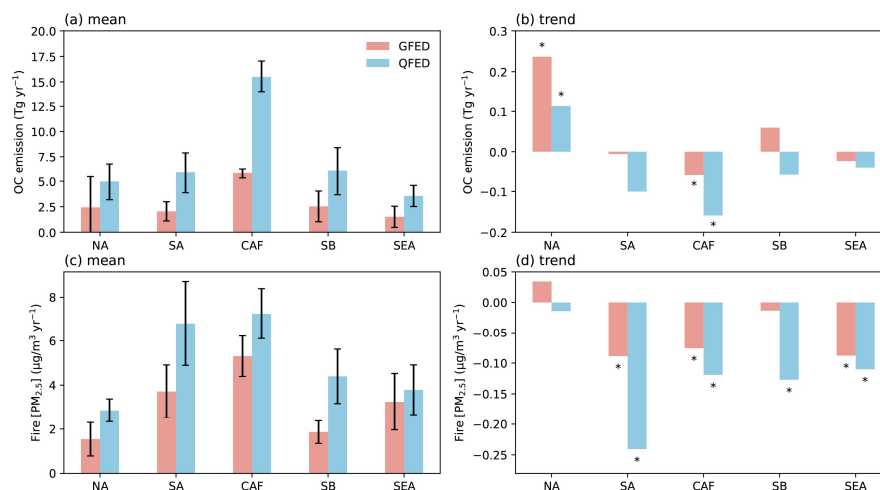
Figure 7. The mean (a) and trend (b) of OC emissions in high fire-prone regions indicated by the GFED (red) and QFED (blue)
560 inventories. Panels (c) and (d) display the fire-sourced [$PM_{2.5}$] predicted using these two inventories. Errorbars represent one
standard deviation for the year-to-year variations, and '*' denotes areas with significant ($p < 0.05$) trends. Domain of the
labelled regions is shown on Fig. 6a.
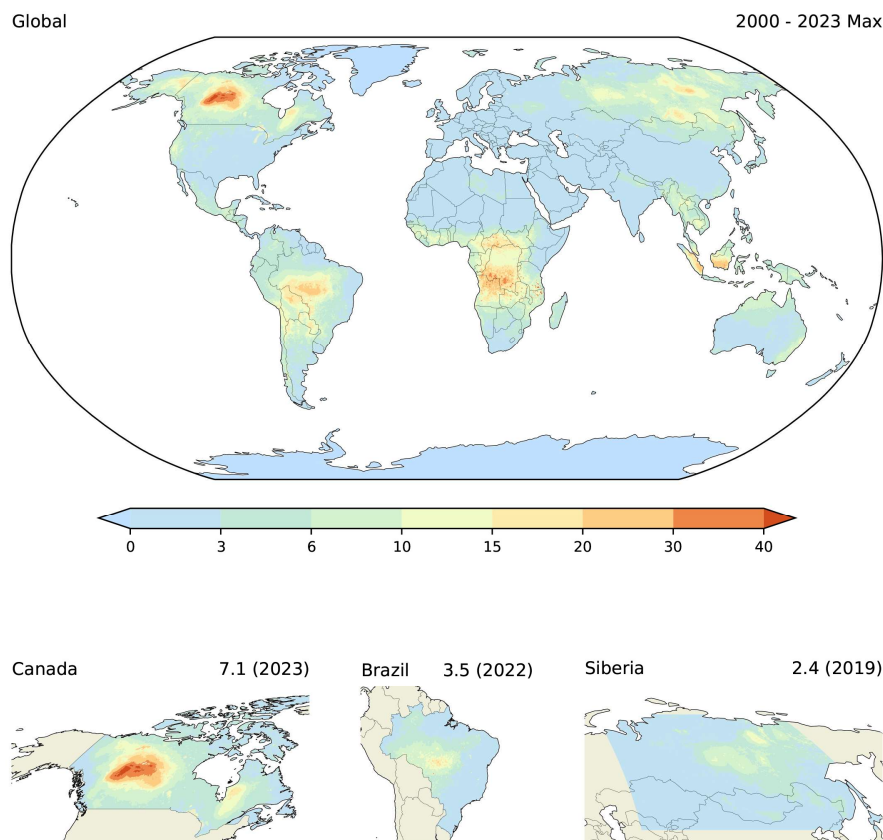
Figure 8. The global maximum of fire [PM$_{2.5}$] (μg m^{-3}) from 2000 to 2023 derived using the GFED inventory, along with fire [PM$_{2.5}$] during years of high wildfire emissions in various regions. For each grid on the global map, the maximum fire-sourced [PM$_{2.5}$] during 2000-2023 is shown. For the three regions, numbers before the parentheses represent the mean fire [PM$_{2.5}$] averaged for the affected countries or regions in that specific year.

570

Table 1. Mean PM$_{2.5}$ before and after bias-correction in selected regions averaged for 2000-2023

		EUS	CE	NAF	IN	EA
	GC	14.38±3.39	24.74±3.67	45.97±16.46	33.73±16.36	68.68±33.41
GFED	XGB	10.42±2.16	15.94±3.33	32.74±8.08	29.59±8.07	40.08±16.73
	Difference	3.96±3.13	8.79±3.85	13.22±10.33	4.14±10.54	28.61±20.14
	GC	16.55±3.44	23.56±3.25	47.56±15.82	35.60±16.30	70.57±32.36
QFED	XGB	10.99±2.58	16.10±3.20	27.09±7.20	28.78±7.07	39.00±16.95
	Difference	5.56±3.38	7.46±3.81	20.47±10.57	6.82±12.90	31.57±19.79

575

Table 2. The mean fire-induced [PM$_{2.5}$] in selected regions averaged for 2000-2023

	NA	SA	CAF	SB	SEA	Global
GFED	1.54±0.98	3.72±2.43	5.31±4.28	1.86±1.08	3.25±1.72	1.94±2.24
QFED	2.86±1.31	6.81±2.77	7.25±4.99	4.40±1.68	3.79±1.72	3.74±2.98